The Astrophysical Journal, 732:32 (13pp), 2011 May 1 doi:10.1088/0004-637X/732/1/32

THE DIVERSITY OF MASSIVE STAR OUTBURSTS. I. OBSERVATIONS OF SN2009ip, UGC 2773 OT2009-1, AND THEIR PROGENITORS

Ryan J. Foley[1,6], Edo Berger[1], Ori Fox[2], Emily M. Levesque[3,7], Peter J. Challis[1], Inese I. Ivans[4], James E. Rhoads[5], and Alicia M. Soderberg[1]

[1] Harvard-Smithsonian Center for Astrophysics, 60 Garden Street, Cambridge, MA 02138, USA; rfoley@cfa.harvard.edu
[2] Department of Astronomy, University of Virginia, P.O. Box 400325, Charlottesville, VA 22904, USA
[3] Institute for Astronomy, University of Hawaii, 2680 Woodlawn Dr., Honolulu, HI 96822, USA
[4] Department of Physics and Astronomy, University of Utah, Salt Lake City, UT 84112, USA
[5] School of Earth and Space Exploration, Arizona State University, P.O. Box 871404, Tempe, AZ 85287, USA
Received 2010 February 2; accepted 2011 February 27; published 2011 April 12

ABSTRACT

Despite both being outbursts of luminous blue variables (LBVs), SN 2009ip and UGC 2773 OT2009-1 have very different progenitors, spectra, circumstellar environments, and possibly physical mechanisms that generated the outbursts. From pre-eruption *Hubble Space Telescope* images, we determine that SN 2009ip and UGC 2773 OT2009-1 have initial masses of $\gtrsim$60 and $\gtrsim$25 $M_{\odot}$, respectively. Optical spectroscopy shows that at peak, SN 2009ip had a 10,000 K photosphere and its spectrum was dominated by narrow H Balmer emission, similar to classical LBV giant outbursts, also known as "supernova impostors." The spectra of UGC 2773 OT2009-1, which also have narrow Hα emission, are dominated by a forest of absorption lines, similar to an F-type supergiant. Blueshifted absorption lines corresponding to ejecta at a velocity of 2000–7000 km s^{-1} are present in later spectra of SN 2009ip—an unprecedented observation for LBV outbursts, indicating that the event was the result of a supersonic explosion rather than a subsonic outburst. The velocity of the absorption lines increases between two epochs, suggesting that there were two explosions in rapid succession. A rapid fading and rebrightening event concurrent with the onset of the high-velocity absorption lines is consistent with the double-explosion model. A near-infrared excess is present in the spectra and photometry of UGC 2773 OT2009-1 that is consistent with ∼2100 K dust emission. We compare the properties of these two events and place them in the context of other known massive star outbursts such as η Car, NGC 300 OT2008-1, and SN 2008S. This qualitative analysis suggests that massive star outbursts have many physical differences that can manifest as the different observables seen in these two interesting objects.

Key words: circumstellar matter – dust, extinction – stars: evolution – stars: individual (SN 2009ip, UGC 2773 OT2009-1) – stars: massive – stars: mass-loss – stars: variables: general – stars: variables: S Doradus – stars: winds, outflows

Online-only material: color figures

1. INTRODUCTION

Very massive stars appear to go through a phase of instability and large mass loss; during this stage, a star is a member of the luminous blue variable (LBV) class (see Humphreys & Davidson 1994 for a review). In addition to low-amplitude variability (called S Dor variability after the prototypical LBV), where the star ejects mass from its envelope but its bolometric luminosity remains nearly constant, some LBVs have "giant eruptions." Giant eruptions can expel $\gtrsim$1 $M_{\odot}$ of material, while having a luminosity similar to the lowest-luminosity supernovae (SNe). The classical examples of giant eruptions are P Cygni in 1600 and η Car in 1843, and more recent, extragalactic examples include SN 1961V (Goodrich et al. 1989; Filippenko et al. 1995; Van Dyk et al. 2002; but see Chu et al. 2004), V12/SN 1954J (Smith et al. 2001; Van Dyk et al. 2005), SN 1997bs (Van Dyk et al. 2000), SN 2000ch (Wagner et al. 2004), and V37/SN 2002 kg (Weis & Bomans 2005; Maund et al. 2006; Van Dyk et al. 2006). Other potential examples exist, but all events listed above have pre-event imaging where the progenitor star has been identified as a probable or definite LBV.

Two examples of a new class of stellar eruptions have recently emerged. The progenitors of NGC 300 OT2008-1 and SN 2008S were both detected in pre-event *Spitzer* images, but were undetected to deep limits in the optical (Prieto et al. 2008; Berger et al. 2009b; Bond et al. 2009; Botticella et al. 2009; Thompson et al. 2009), indicating significant reddening from circumstellar dust. The progenitor stars were originally believed to have ZAMS masses of 8–20 $M_{\odot}$, which is below that of the least massive LBVs. Using the stars in the vicinity of NGC 300 OT2008-1, Gogarten et al. (2009) found a slightly higher mass range of 12–25 $M_{\odot}$. A reasonable range for the initial mass of the progenitors is ∼10–25 $M_{\odot}$, with NGC 300 OT2008-1, having a more luminous progenitor, being toward the upper end of that range. Thompson et al. (2009) investigated these objects in the context of other similar events and the detection of similar progenitor stars in M33. They determine that the rate of such events is relatively high, but the number of potential progenitors is relatively small, indicating a short-lived extremely dusty stage of stellar evolution; however, that conclusion assumes a single outburst per progenitor.

Recently, two transients were discovered with one being very similar to classical LBV giant eruptions (SN 2009ip) and another sharing characteristics of both LBV giant eruptions and the outbursts of the dusty stars discussed above (UGC 2773

[6] Clay Fellow.
[7] Predoctoral Fellow, Smithsonian Astrophysical Observatory.

OT2009-1). SN 2009ip was discovered by Maza et al. (2009) in NGC 7259 ($\mu = 32.05 \pm 0.15$ mag[8]; $D \approx 24$ Mpc) on 2009 August 26 (UT dates will be used throughout this paper).

Smith et al. (2010, hereafter S10) presented an extensive analysis of these two transients. They noted that SN 2009ip had been variable for several years and identified a possible progenitor with $M_{\rm F606W} \approx -10.1$ mag, in an archival *Hubble Space Telescope* (*HST*) image. The variability, high luminosity, and additional spectroscopic data led them to suggest that SN 2009ip was an LBV outburst. An early spectrum of the event showed a blue continuum with relatively narrow (FWHM = 550 km s^{-1}) H Balmer lines. The combination of the spectrum with the relatively low absolute magnitude ($R \approx -13.7$ mag) led us to also conclude that SN 2009ip was an LBV giant eruption (Berger et al. 2009a). The transient underwent extreme variability shortly after maximum,[9] fading by at least 3 mag in 16 days and rebrightening by 2 mag in the next 10 days S10, reminiscent of the variability immediately before maximum of the 1843 eruption of η Car (e.g., Humphreys et al. 1999; Frew 2004) and immediately after maximum in the LBV outburst SN 2000ch (Wagner et al. 2004). S10 presented a historical light curve of SN 2009ip that begins 5 years before maximum light, excluding the *HST* image of the progenitor. The star varied by at least 1.5 mag during this time. S10 presented additional data which led them to conclude that SN 2009ip was the giant eruption of a 50–80 $M_\odot$ LBV.

UGC 2773 OT2009-1 was discovered by Boles (2009) in UGC 2773 ($\mu = 28.82 \pm 0.17$ mag; $D \approx 6$ Mpc) on 2009 August 18. It was originally reported as a possible SN. We obtained a spectrum and noted that it had a peculiar spectrum with relatively narrow (FWHM = 350 km s^{-1}) Hα emission, P-Cygni lines from the Ca II NIR triplet, and [Ca II] emission lines (Berger & Foley 2009). We also noted that the spectrum was similar to that of NGC 300 OT2008-1 and mentioned that it was possibly a very low luminosity SN II or an LBV outburst, "but the strong [Ca II] emission would be unexpected in this case." Berger & Foley (2009) also detected a potential progenitor star in archival *HST* images. S10 presented a historical light curve of UGC 2773 OT2009-1 that begins nine years (excluding the *HST* image of the progenitor) before maximum light. The star slowly increased from F814W = 22.22 mag to an unfiltered magnitude of 17.70 mag at maximum light, corresponding to a linear increase of $\sim$0.4 mag yr^{-1} before outburst. They also noted that the event had a spectrum similar to an F-type supergiant. S10 concluded from the progenitor identification, their historic light curve, the peak luminosity, optical light curves, and spectra that UGC 2773 OT2009-1 was the outburst of a $\gtrsim$20 $M_\odot$ LBV.

This is the first in a series of papers where we investigate the diversity of massive star outbursts. In this paper, we demonstrate the heterogeneity of the class with observations of SN 2009ip and UGC 2773 OT2009-1. In future papers, we will detail the properties of the class and the links between observations and the physical mechanisms which cause the outbursts. Throughout this paper, we confirm several finding of S10. Although our interpretation is very similar, there are a few instances where we differ. In Section 2, we present ultraviolet (UV), optical, and near-infrared (NIR) photometry and optical and NIR spectroscopy of UGC 2773 OT2009-1 and SN 2009ip. In this section, we also refine previous identifications of the progenitors. In Section 3, we examine the progenitor masses, the spectroscopic characteristics of the outbursts, and the spectral energy distributions (SEDs) of the events. In Section 4, we discuss how these outbursts connect to previous massive star outbursts and the mass loss history and ultimate fates of massive stars. We summarize our conclusions in Section 5.

2. OBSERVATIONS AND DATA REDUCTION

2.1. Identification and HST Photometry of the Progenitors

UGC 2773 was observed with *HST*/WFPC2 on 1999 August 14 (Program 8192; PI: Seitzer). The observations included two exposures of 600 s each with the F606W and F814W (roughly *V* and *I*) filters. NGC 7259 was observed with *HST*/WFPC2 on 1999 June 29 (Program 6359; PI: Stiavelli). Exposures of 200 and 400 s were obtained with the F606W filter.

To determine whether the progenitors of SN 2009ip and UGC 2773 OT2009-1 are detected in the archival *HST* observations, we performed differential astrometry using optical observations of the transients. Observations of UGC 2773 OT2009-1 were obtained with the Gemini Multi-Object Spectrograph (GMOS) on the Gemini-North 8 m telescope, and the astrometry was performed using 55 objects in common with the *HST*/WFPC2 images resulting in an astrometric rms of $\sigma_{\rm GB\rightarrow HST} = 24$ mas in each coordinate. Observations of SN 2009ip were obtained with the Inamori Magellan Areal Camera and Spectrograph (IMACS) on the Magellan/Baade 6.5 m telescope, and the astrometry was performed using 10 objects in common with the *HST*/WFPC2 image resulting in an astrometric rms of $\sigma_{\rm GB\rightarrow HST} = 38$ mas in each coordinate.

The positions of the two transients on the archival *HST* images are shown in Figure 1. In both cases, we find a clear coincidence with objects in the archival *HST* images. For SN 2009ip we find an offset of 24 ± 38 mas relative to the object in the WFPC2/F606W image, while for UGC 2773 OT2009-1 we find an offset of 32 ± 24 mas relative to the object in the WFPC2/F606W and F814W images.

The measurements of the photometry for UGC 2773 OT2009-1 and nearby stars were done using HSTphot 1.1 (Dolphin 2000). HSTphot was run using a weighted PSF-fit, which is recommended for crowded fields, and a local sky determination, which is recommended for rapidly varying backgrounds. HSTphot performs the conversion from *HST*/WFPC2 flight magnitudes to the Bessel magnitude system. Our astrometry and photometry for the nominal progenitor of UGC 2773 OT2009-1 and nearby stars are listed in Table 1.

We performed photometry of the point source coincident with SN 2009ip using a 0.″5 aperture and a zero point of 22.47 mag appropriate for the F606W filter. We further applied a correction of -0.29 mag to convert to the Vega system and applied a correction for the Galactic extinction of 0.05 mag. The resulting magnitude of the source is 21.84 ± 0.25 mag. For reasonable colors (see Section 3.1.1), this corresponds to $M_V = -10.3 \pm 0.3$ mag. We note that there is a potential systematic offset of 0.5 mag in the absolute magnitude that corresponds to the assumed distance modulus (see Footnote 8).

[8] We use the distance modulus corresponding to the Hubble distance for NGC 7259 with $H_0 = 73$ km s^{-1} Mpc^{-1} and correcting for the Virgo Infall and Great Attractor flow model of Mould et al. (2000). Smith et al. (2010) use a distance modulus of 31.55 mag, which differs by 0.50 mag from our assumed value, corresponding to the Hubble-flow distance modulus correcting only for the CMB dipole.

[9] To be consistent with S10, we adopt MJD = 55061.5 and MJD = 55071.75 as times of maximum light for UGC 2773 OT2009-1 and SN 2009ip, respectively. However, we note that the objects may reach their true maximum later, which UGC 2773 OT2009-1 already has (as shown by data presented in S10).

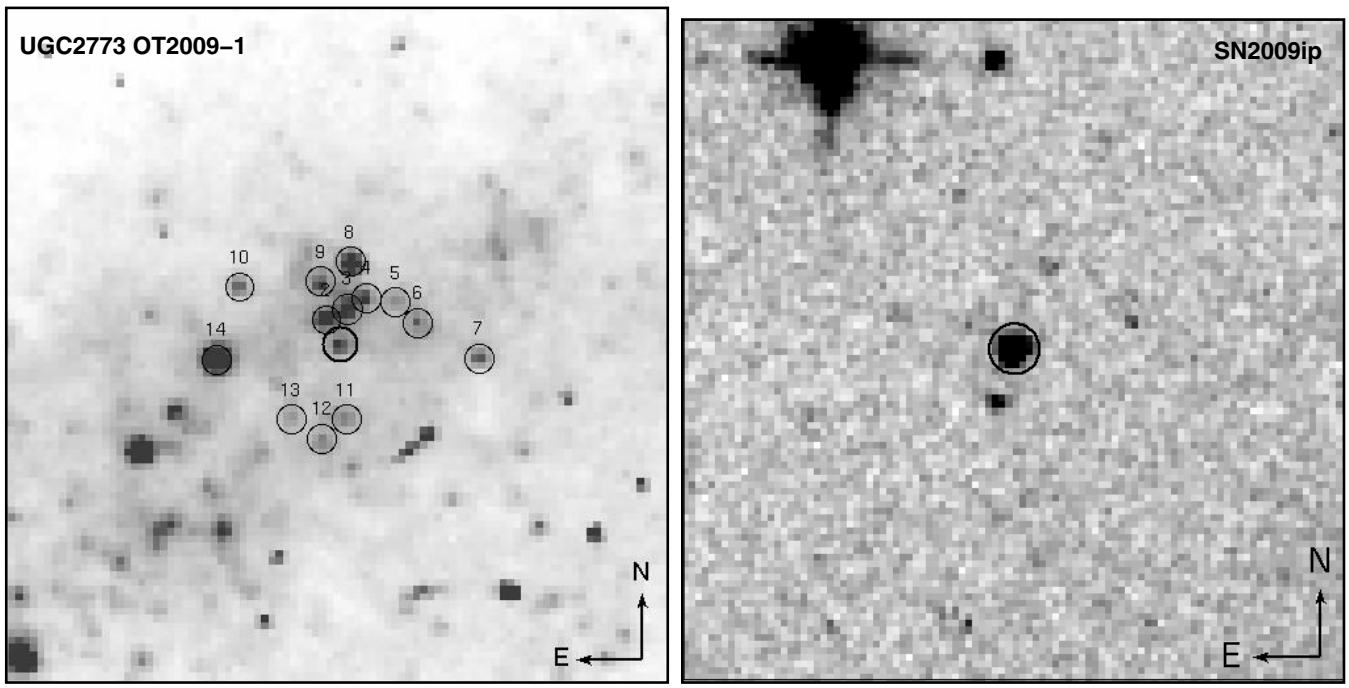

Figure 1. *HST*/WFPC2 F606W image at the position of UGC 2773 OT2009-1 (left) and SN 2009ip (right) obtained 10 years before maximum. Both images are $10'' \times 10''$, and north is up and east is left. The UGC 2773 OT2009-1 and SN 2009ip images have pixel scales of $0.1''$pixel^{-1}. The position of each transient is marked by the black circle whose radius corresponds to 10σ uncertainty in the position.

Table 1
HST Photometry of Stars Near UGC 2773 OT2009-1

Object	R.A.	Decl.	F606W (mag)	F814W (mag)
1[a]	03:32:7.240	+47:47:39.60	22.824 (0.032)	22.286 (0.053)
2	03:32:7.258	+47:47:39.99	22.474 (0.027)	22.164 (0.050)
3	03:32:7.229	+47:47:40.14	22.672 (0.036)	22.222 (0.054)
4	03:32:7.203	+47:47:40.29	22.853 (0.035)	22.591 (0.081)
5	03:32:7.162	+47:47:40.23	23.864 (0.072)	22.729 (0.074)
6	03:32:7.132	+47:47:39.94	23.413 (0.051)	22.748 (0.092)
7	03:32:7.048	+47:47:39.45	22.925 (0.034)	20.956 (0.020)
8	03:32:7.225	+47:47:40.79	21.724 (0.016)	21.043 (0.022)
9	03:32:7.266	+47:47:40.51	23.007 (0.039)	22.548 (0.067)
10	03:32:7.377	+47:47:40.44	22.967 (0.035)	21.682 (0.035)
11	03:32:7.230	+47:47:38.60	23.762 (0.092)	23.182 (0.113)
12	03:32:7.263	+47:47:38.34	23.578 (0.058)	23.095 (0.100)
13	03:32:7.306	+47:47:38.61	24.015 (0.081)	23.304 (0.116)
14	03:32:7.409	+47:47:39.44	21.194 (0.026)	19.934 (0.017)

Note. [a] Star 1 is identified as the progenitor of UGC 2773 OT2009-1.

Table 2
UV and Optical Photometry of UGC 2773 OT2009-1 and SN 2009ip

Object	MJD	Filter	Mag	Telescope
UGC 2773 OT2009-1	51404.13	F606W	22.82 (0.03)	*HST*
UGC 2773 OT2009-1	51404.14	F814W	22.29 (0.05)	*HST*
UGC 2773 OT2009-1	55078.38	*J*	15.47 (0.06)	Fan Mountain
UGC 2773 OT2009-1	55078.40	*H*	14.99 (0.06)	Fan Mountain
UGC 2773 OT2009-1	55078.39	K_s	14.63 (0.07)	Fan Mountain
UGC 2773 OT2009-1	55078.53	*g*	18.32 (0.01)	Gemini-North
UGC 2773 OT2009-1	55078.53	*r*	17.22 (0.01)	Gemini-North
UGC 2773 OT2009-1	55078.53	*i*	16.68 (0.01)	Gemini-North
UGC 2773 OT2009-1	55089.31	*J*	15.47 (0.06)	Fan Mountain
UGC 2773 OT2009-1	55089.32	*H*	14.91 (0.07)	Fan Mountain
UGC 2773 OT2009-1	55089.33	K_s	14.91 (0.09)	Fan Mountain
SN 2009ip	51358.50	F606W	21.84 (0.17)	*HST*
SN 2009ip	55084.44	UVW2	21.09 (0.19)	*Swift*
SN 2009ip	55084.45	UVM2	20.92 (0.28)	*Swift*
SN 2009ip	55084.44	UVW1	20.69 (0.18)	*Swift*
SN 2009ip	55084.44	*U*	20.29 (0.16)	*Swift*
SN 2009ip	55084.44	*B*	20.64 (0.09)	*Swift*
SN 2009ip	55084.45	*V*	20.47 (0.37)	*Swift*

The stars we have identified as the progenitors are the same as those reported by Miller et al. (2009), Berger & Foley (2009), and S10. Additionally, our photometry of the progenitors is consistent with that of S10.

2.2. Ultraviolet, Optical, and Near-infrared Photometry

We obtained optical photometry of UGC 2773 OT2009-1 with the Gemini Multi-Object Spectrograph (GMOS) on the Gemini-North 8 m telescope in the *gri* filters. We performed the photometry using IRAF/`phot` with the standard GMOS zero-points.[10] Our results are presented in Table 2.

We obtained near-infrared (NIR) photometry of UGC 2773 OT2009-1 with FanCam, a 1024 × 1024 HAWAII-I HgCdTe imaging system on the University of Virginia's 31 inch telescope at Fan Mountain, just outside of Charlottesville, VA (Kanneganti et al. 2009). Each epoch consists of fifteen minutes of integration in JHK_s bands, which have detection limits at the 10σ level of 0.066, 0.098, and 0.156 mJy (or 18.5, 17.5, and 16.5 mag), respectively. Individual exposures are sky-background-limited and have an integration time of either 30 or 60 s. Flat-field frames are composed of dusk and dawn sky observations. We employed standard NIR data reduction techniques in IRAF.[11] Because of the relatively small galaxy size, it was possible to

[10] http://www.gemini.edu/sciops/instruments/gmos/imaging

[11] IRAF is distributed by the National Optical Astronomy Observatory, which is operated by the Association of Universities for Research in Astronomy, Inc., under cooperative agreement with the National Science Foundation.

fit the entire galaxy in a single array quadrant. Empty quadrants were efficiently utilized as sky exposures. Data were taken with the galaxy placed in each quadrant and each quadrant was reduced separately. Ultimately, all reduced quadrants were co-added. We performed photometry with IRAF's PSF package. For magnitude calibration, the transient is compared to 2MASS reference stars located in the field of view. Table 2 lists our JHK_s photometry, which is similar to the single epoch JHK_s data from S10.

We obtained UV and optical observations of SN 2009ip with the *Swift* UV/optical telescope on 2009 September 10. The data were processed using standard routines within the HEASOFT package. Photometry of the transient in all filters, with the exception of UVW2, was performed using a 2″ aperture to avoid contamination from nearby objects. Aperture corrections to the standard 5″ aperture were determined using isolated stars; photometry of the source in the UVW2 filter was performed using a 5″ aperture.

2.3. X-ray Observations

We observed SN 2009ip and UGC 2773 OT2009-1 with the *Swift* X-ray Telescope on 2009 September 10 for a total exposure time of 9.0 and 4.2 ks, respectively. No X-ray counterpart is detected at the position of either source to a limit of $F_X \lesssim 2.8 \times 10^{-14}$ and $\lesssim 1.1 \times 10^{-13}$ erg s^{-1} cm^{-2}, respectively (95% limit). In both cases we assume a power-law model with an electron index of -2, and account for the Galactic neutral hydrogen column. The corresponding limits on the luminosity are $L_X \lesssim 1.9 \times 10^{39}$ and $\lesssim 4.8 \times 10^{38}$ erg s^{-1}. These limits are comparable to the X-ray emission from SNe on a similar timescale (e.g., Soderberg et al. 2008).

2.4. Radio Observations

We observed both events with the Very Large Array[12] (VLA) following their optical discovery to search for radio counterparts, under Rapid Response programs AS1001 and AS1002 (PI: Soderberg). Our radio observations were carried out at two frequencies, 8.46 and 22.5 GHz, on dates spanning 2009 September 7.36–16.51 in the C-array antenna configuration. All observations were taken in standard continuum observing mode with a bandwidth of 2 × 50 MHz. Phase referencing was performed with calibrators J0325+469 and J2213-254, and we used 3C38 (J0137+331) for flux calibration. Data were reduced using standard packages within the Astronomical Image Processing System (AIPS).

We detect no radio sources in positional coincidence with either object and derive upper limits summarized in Table 3. At 8.5 GHz, our upper limits[13] correspond to $L_\nu < 1.3 \times 10^{26}$ erg s^{-1} Hz^{-1} and $L_\nu < 2.6 \times 10^{24}$ erg s^{-1} Hz^{-1} for SN 2009ip and UGC 2773 OT2009-1, respectively. These limits are less luminous than an extrapolation of the observed SN 1961V radio emission at $t \approx 10$ yr, to a similarly early epoch as $L_\nu \propto t^{-1.75}$ (Stockdale et al. 2001). We note, however, that the SN 1961V radio emission may have reached maximum intensity significantly later than our observations of UGC 2773 OT2009-1 and SN 2009ip, similar to the radio evolution of SNe IIn which typically reach maximum light several years after the explosion (van Dyk et al. 1996).

[12] The Very Large Array is operated by the National Radio Astronomy Observatory, a facility of the National Science Foundation operated under cooperative agreement by Associated Universities, Inc.

[13] Upper limits are calculated as the measured flux density at the optical position summed with 2× rms the off-source map noise.

Table 3
VLA Observations of UGC 2773 OT2009-1 and SN 2009ip

Object	Date (UT)	$F_{\nu,8.5}$ (μJy)	$F_{\nu,22}$ (μJy)
SN 2009ip	2009 Sep 7.36	...	-122 ± 243
...	2009 Sep 9.24	67 ± 47	...
UGC 2773 OT2009-1	2009 Sep 13.57	...	-57 ± 66
...	2009 Sep 16.51	11 ± 27	...

Note. Uncertainties are 1σ rms map noise.

A comparison of these radio upper limits for the outbursts to the observed properties of other core-collapse SNe places them among the least luminous events, 2–4 orders of magnitude less luminous than the most powerful SNe IIn, and 4–200 times higher than the early radio signal seen for SN 1987A (Ball et al. 1995). Through this simple comparison we emphasize that radio data alone cannot distinguish between massive star outbursts and catastrophic explosions.

2.5. Optical Spectroscopy

We obtained low- and medium-resolution spectra of SN 2009ip and UGC 2773 OT2009-1 with the MagE spectrograph (Marshall et al. 2008) and LDSS3 spectrograph[14] on the Magellan Clay 6.5 m telescope, the Blue Channel spectrograph (Schmidt et al. 1989) on the MMT 6.5 m telescope, and GMOS (Hook et al. 2004) on the Gemini-North 8 m telescope. A journal of our optical spectroscopic observations can be found in Table 4.

Standard CCD processing and spectrum extraction were accomplished with IRAF. The data were extracted using the optimal algorithm of Horne (1986). Low-order polynomial fits to calibration-lamp spectra were used to establish the wavelength scale, and small adjustments derived from night-sky lines in the object frames were applied. For the MagE spectra, the sky was subtracted from the images using the method described by Kelson (2003). The GMOS data were reduced using the Gemini IRAF package (for details, see Foley et al. 2006). We employed our own IDL routines to flux calibrate the data and remove telluric lines using the well-exposed continua of the spectrophotometric standards (Wade & Horne 1988; Foley et al. 2003, 2009).

Representative spectra of SN 2009ip and UGC 2773 OT2009-1 are presented in Figure 2. Both objects have similar blue continua, but the line features are very different. SN 2009ip has few line features besides strong H Balmer lines, Na D, and He I. Although UGC 2773 OT2009-1 has a strong Hα line, it is much narrower and weaker than that of SN 2009ip. UGC 2773 OT2009-1 also displays many additional narrow line features, including lines from intermediate mass and Fe-group elements. Blueward of ∼5500 Å, UGC 2773 OT2009-1 is dominated by a forest of Fe II lines. Finally, UGC 2773 OT2009-1 has very strong Ca II NIR triplet lines and [Ca II] λλ7291, 7324 lines. These features are rarely seen in classical LBV outbursts (and [Ca II] has never been seen in one), but were distinguishing features of SN 1999bw (Garnavich et al. 1999), SN 2008S (e.g., Smith et al. 2009), and NGC 300 OT2008-1 (e.g., Bond et al. 2009; Berger et al. 2009b).

The spectra from 2009 September 21 (corresponding to days 34 and 24 for UGC 2773 OT2009-1 and SN 2009ip,

[14] http://www.lco.cl/telescopes-information/magellan/instruments-1/ldss-3-1/

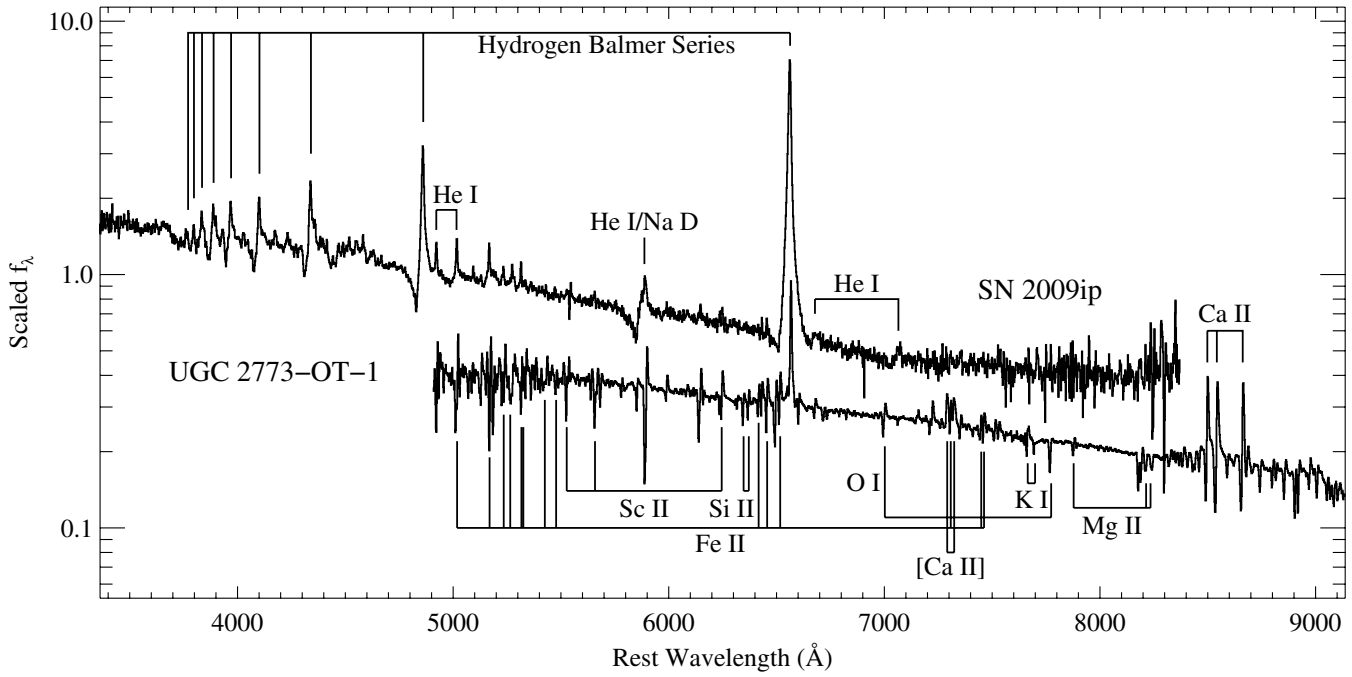

Figure 2. Optical spectra of SN 2009ip and UGC 2773 OT2009-1. The spectrum of UGC 2773 OT2009-1 has been dereddened by $E(B-V) = 0.564$ mag. Several lines are identified and marked.

Table 4
Log of Optical Spectral Observations

Phase[a]	UT Date	Telescope/ Instrument	Grating/Grism/ Central Wavelength (Å)	Exposure (s)	Observer[b]
15.1	2009 Sep 2.6	Gemini/GMOS	R400/7000	2 × 1200	KO, RM
32.9	2009 Sep 20.4	MMT/Blue Channel	300/5787	3 × 1200	PC
33.9	2009 Sep 21.4	MMT/Blue Channel	300/5787	1200	PC
33.9	2009 Sep 21.4	MMT/Blue Channel	832/4029	2 × 900	PC
34.0	2009 Sep 21.5	MMT/Blue Channel	832/4830	2 × 900	PC
34.0	2009 Sep 21.5	MMT/Blue Channel	832/6563	3 × 900	PC
95.8	2009 Nov 22.3	MMT/Blue Channel	300/5787	2 × 1800	PC
3.5	2009 Sep 1.3	Clay/MagE	···	3 × 900	II
22.5	2009 Sep 20.3	MMT/Blue Channel	300/5787	4 × 1200	PC
23.5	2009 Sep 21.2	MMT/Blue Channel	832/4029	2 × 1200	PC
23.5	2009 Sep 21.3	MMT/Blue Channel	832/4830	2 × 1200	PC
23.5	2009 Sep 21.3	MMT/Blue Channel	832/6563	1200	PC
85.6	2009 Nov 22.1	MMT/Blue Channel	300/5787	3 × 1200	PC
252.6	2010 May 8.4	Clay/LDSS3	VPH-ALL	2 × 1200	EB, RC

Notes.
[a] Days since maximum, MJD 55,061.5 and 55,071.8 for UGC 2773 OT2009-1 and SN 2009ip (S10), respectively.
[b] EB: E. Berger; II: I. Ivans; KO: K. Olsen; PC: P. Challis; RC: R. Chornock; RM: R. McDermid.

respectively) were obtained on the same night as the LRIS spectra shown by S10.

Our late-time spectrum of SN 2009ip, taken 253 days after maximum is very similar to our 86 day spectrum. The key differences is that the equivalent widths of the Balmer lines have decreased by ∼50% and their widths have increased (see Section 3.3.1).

2.6. Near-infrared Spectroscopy

On 2009 September 9 (22 days after maximum), we obtained a 2400 s NIR spectrum of UGC 2773 OT2009-1 with TripleSpec, a medium resolution NIR spectrograph located at Apache Point Observatory. This spectrograph is one of three NIR, cross-dispersed spectrographs covering wavelengths from 1 to 2.4 μm simultaneously at a resolution of ∼3500 (Wilson et al. 2004; Herter et al. 2008). We collected eight, 300 s sky-background-limited exposures, for a total integration time of 2400 s. We extracted the spectrum with a modified version of the IDL-based SpexTool (Cushing et al. 2004). This tool removes any contribution from the underlying galactic arm by fitting the background with a 2nd order polynomial.

3. RESULTS

3.1. Progenitor Masses

3.1.1. SN 2009ip

We use the absolute magnitude, $M_V = -10.3 \pm 0.3$ mag, of the progenitor of SN 2009ip, along with an estimated range

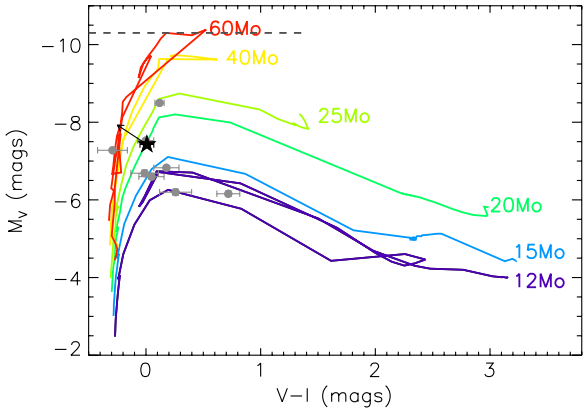

Figure 3. Color–magnitude diagram ($V-I$ vs. M_V) for the progenitor of UGC 2773 OT2009-1 (star) and stars spatially located within the same star cluster (gray circles). The measurements have been corrected for the Milky Way extinction of $A_V = 1.75$ mag and $E(V-I) = 0.902$ mag, but no host or circumstellar extinction is assumed for the stars. For comparison, solar metallicity, non-rotating, "standard" mass loss stellar evolution tracks are also plotted (Schaller et al. 1992). The progenitor of UGC 2773 OT2009-1 has the same colors and absolute magnitude of a 20 $M_\odot$ model. The stars in the cluster are consistent with the models of stars with ZAMS masses $\leqslant$25 $M_\odot$, but a single star is also consistent with a much higher mass. The arrow represents $A_V = 0.5$ mag of additional extinction (assuming $R_V = 3.1$). The dashed line represents the absolute magnitude of the progenitor of SN 2009ip with a reasonable range of colors. The luminosity of the progenitor of SN 2009ip is consistent with an initial mass of $\gtrsim$60 $M_\odot$.

(A color version of this figure is available in the online journal.)

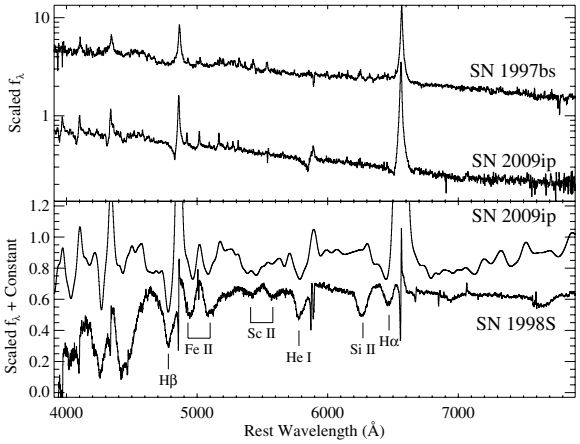

Figure 4. Top panel: the 23 day optical spectrum of SN 2009ip compared to the 2 day spectrum of SN 1997bs (Van Dyk et al. 2000). Bottom panel: the 86 day optical spectrum of SN 2009ip after smoothing and subtracting a 10,000 K blackbody (see the text for details). For comparison, the 25 day spectrum of SN 1998S (after subtracting a 10,000 K blackbody) is also shown (Leonard et al. 2000). Prominent, high-velocity lines have been marked.

of $V-I$ colors of -0.05 to 1.4 mag (representative of LBV colors spanning from O to F spectral types), to plot it as a line on a color–magnitude diagram (Figure 3). For this progenitor we find a Milky Way extinction of $E(B-V) = 0.019$ mag ($A_V = 0.05$ mag; Schlegel et al. 1998). We adopt a distance modulus of $\mu = 32.05$ mag for NGC 7259 (see discussion in Section 1), and assume no additional host galaxy or circumstellar extinction.

In Figure 3, we compare the color of the SN 2009ip progenitor to the non-rotating, standard mass-loss evolutionary tracks of the Geneva group (Schaller et al. 1992). From this plot we can place a lower initial mass limit of 60 $M_\odot$ on the progenitor of SN 2009ip in the absence of a color estimate for this progenitor, the higher-mass evolutionary tracks all coincide with its estimated location on the color–magnitude diagram, precluding us from placing an upper limit on this initial mass estimate. Figure 3 assumes a solar metallicity for these tracks; however, we find that our progenitor mass prediction is consistent across the full range of metallicities accommodated by the Geneva evolutionary tracks ($Z = 0.05\,Z_\odot$ to $Z = 2\,Z_\odot$). It should be noted that an increased amount of extinction, from the host galaxy or circumstellar environment, could also effectively increase the estimated initial mass of this progenitor.

S10 estimated the initial mass for the progenitor of SN 2009ip to be 50–80 $M_\odot$. Although the *HST* photometry from S10 is the same as that presented here, their assumed distance modulus is 0.50 mag smaller than our assumed value. They also make no color correction to transform the F606W measurements into V. Despite these differences, the two mass ranges are nearly identical.

3.1.2. UGC 2773 OT2009-1

Using its M_V and $V-I$ color, we are able to determine an estimate of the initial mass for the progenitor of UGC 2773 OT2009-1 (Figure 3). There is significant Milky Way extinction of $E(B-V) = 0.564$ mag ($A_V = 1.75$ mag; Schlegel et al. 1998), which we convert to $E(V-I) = 0.902$ mag (Schultz & Wiemer 1975). We use a distance modulus of $\mu = 28.82$ mag and initially assume no host galaxy or circumstellar extinction.

From Figure 3, we find that the progenitor of UGC 2773 OT2009-1 is consistent with an initial mass of $\sim$20 $M_\odot$. Our progenitor mass prediction remains the same across the full range of metallicities covered by the Geneva evolutionary tracks and is consistent with the value found by S10.

We have also performed this procedure on several stars in the vicinity of the progenitor of UGC 2773 OT2009-1. Assuming that all of these stars are part of a cluster and were formed at the same time, they should place additional limits on the current maximum-mass stars of the cluster. These stars are all consistent with an initial mass of $M_\odot \lesssim 25\,M_\odot$. There is a single star that is particularly blue (and therefore potentially very massive), but it is still consistent with an initial mass of 25 $M_\odot$. The likely association of the progenitor of UGC 2773 OT2009-1 with this cluster and its upper mass limit of $\sim$25 $M_\odot$ further supports the initial mass estimate for the progenitor of UGC 2773 OT2009-1.

Considering the blue colors of the stars in the cluster, it is unlikely that they are significantly reddened by host galaxy dust. As shown in Figure 3, a relatively small amount of extinction could significantly increase our initial mass estimate for UGC 2773 OT2009-1. In Section 3.4, we show that there was likely a significant amount of circumstellar dust existing before the outburst, indicating that the progenitor had an initial mass much larger than the reddening-free estimate of 20 $M_\odot$.

The combination of the reddening-free initial mass estimate for the progenitor of UGC 2773 OT2009-1, the initial mass estimates of stars likely within the same cluster as the progenitor, and the probably circumstellar dust extinction give us a conservative lower limit on the initial mass of the progenitor of UGC 2773 OT2009-1 of $\sim$25 $M_\odot$. Again, this is nearly identical to the mass limit given by S10.

3.2. Spectroscopic Comparisons

3.2.1. SN 2009ip

We present the 24 and 86 day spectra of SN 2009ip in Figure 4. In the upper panel of Figure 4, the 24 day spectrum is compared to the 2 day spectrum of the LBV outburst SN 1997bs (Van

Dyk et al. 2000). Both objects have blue continua, strong and narrow H Balmer lines, and He I and Fe II emission lines. Unlike SN 1997bs, SN 2009ip has a particularly strong He I λ5876 line (with some possible contribution from Na D), and all H Balmer lines and He I λ5876 show strong absorption features with minima blueshifted by ∼3000 km s^{-1} (see Section 3.3.1 for a detailed discussion of this high-velocity absorption).

We have reduced our spectra with many different extraction regions and backgrounds, with the high-velocity absorption features are present in all reductions. The same feature is present in all spectra taken with the MMT on days 23 and 24, which were taken with different gratings and wavelength regions. It is also present on day 86, but with a different velocity. The absorption is present for all Balmer lines and He I λ5876. S10 concurrently detected the high-velocity absorption features, giving additional strength to the existence of the features.

The bottom panel of Figure 4 displays the spectra of SN 2009ip and SN IIn 1998S (after subtracting a 10,000 K blackbody spectrum from both) from 86 and 25 days, respectively. An inverse-variance weighted Gaussian filter (with a width of 1000 km s^{-1}) has been applied to the spectrum of SN 2009ip (Blondin et al. 2006). This filtering will smear out features with intrinsic widths less than 1000 km s^{-1}, but will appropriately smooth features on larger scales. The high-velocity absorption in the 86 day spectrum of SN 2009ip is at a *higher* velocity than at 24 days. At this epoch, the velocity of the fast-moving SN 2009ip ejecta are very similar to that of SN 1998S. Although the H Balmer emission lines are much stronger in SN 2009ip, most other features are similar in the two spectra. In particular, SN 2009ip shows the H Balmer, He I, Sc II, and Fe II features seen in SN 1998S. SN 2009ip is missing the strong absorption at 6250 Å that is attributed to Si II in SN 1998S (Leonard et al. 2000). This feature may be the result of a significant amount of nuclear burning, and thus not present in the ejecta of SN 2009ip.

The high-velocity absorption feature is not present in our spectrum from 253 days, despite it having a comparable signal-to-noise ratio as the other spectra. It is likely that by this point the ejecta have become nebular, and similar to an SN II at late time, the P-Cygni absorptions are no longer visible.

3.2.2. UGC 2773 OT2009-1

As discussed in Section 2.5, UGC 2773 OT2009-1 has a spectrum with narrow Hα emission, [Ca II] emission, and P-Cygni absorption from many intermediate-mass and Fe-group elements. Perhaps the most distinguishing feature compared to other massive star outbursts is the [Ca II] emission. In Figure 5, we compare the 15 day spectrum of UGC 2773 OT2009-1 to spectra of the low-luminosity transients NGC 300 OT2008-1 (Berger et al. 2009b) and SN 2008S (Smith et al. 2009), as well as SN IIn 1994W (Chugai et al. 2004); all of these objects have [Ca II] emission in their spectra.

All spectra in Figure 5 are relatively similar. The continuum of each spectrum is well described by a blackbody spectrum, with all four objects having a similar temperature. Each object has a prominent Hα emission line, with UGC 2773 OT2009-1 having a narrower line than the other objects. Additionally, SN 1994W has a strong Hα absorption line blueward of its emission peak.

NGC 300 OT2008-1 and SN 2008S are very similar objects with massive (10–25 $M_\odot$), dusty progenitors (Prieto 2008; Prieto et al. 2008; Berger et al. 2009b; Bond et al. 2009; Botticella et al. 2009). Smith et al. (2009) first noticed the similarities of the spectra of these objects with those of the yellow

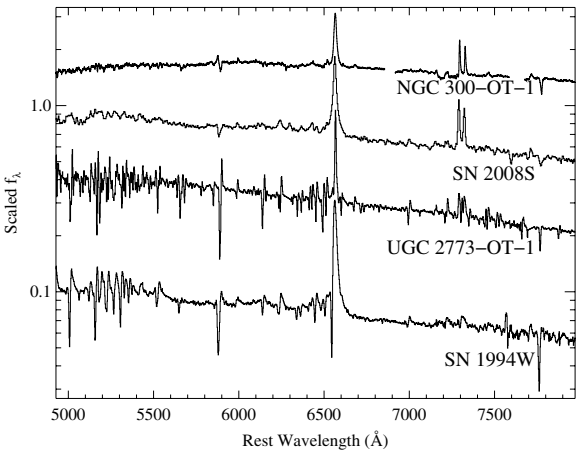

Figure 5. Optical spectra of UGC 2773 OT2009-1, NGC 300 OT2008-1 (Berger et al. 2009b), SN 1994W (Chugai et al. 2004), and SN 2008S (Smith et al. 2009). All spectra have narrow Hα and [Ca II] emission; however, NGC 300 OT2008-1 and SN 2008S lack the forest of lines (especially Fe II) that UGC 2773 OT2009-1 and SN 1994W display.

hypergiant IRC+10240 (e.g., Jones et al. 1993; Humphreys et al. 2002). Although UGC 2773 OT2009-1 shares some spectroscopic properties with these two transients and IRC+10240 (see S10 for additional discussion), the latter objects lack the forest of absorption lines in UGC 2773 OT2009-1. These lines are reminiscent of an F-type supergiant. The P-Cygni profiles of these lines and the hydrogen Balmer emission are very similar to S Dor (e.g., Massey 2000) or other LBVs (e.g., Humphreys & Davidson 1994) during a cool phase.

SN 1994W was very luminous at peak ($M_V \approx -19$ mag), but generated at most 0.03 $M_\odot$ of ^{56}Ni (Sollerman et al. 1998). Dessart et al. (2009) presented an alternative method of producing the photometric and spectroscopic properties of this object: the collision of two massive hydrogen shells ejected from the star with no core collapse. Spectra of SNe IIn are rather heterogeneous (see Figure 5 of Smith et al. 2010 for a comparison of various objects), and SN 1994W is relatively distinct for its narrow absorption features. Given the spectral similarity between UGC 2773 OT2009-1 and SN 1994W, the strict upper limit of ^{56}Ni mass in SN 1994W, and the alternative model of Dessart et al. (2009), one must further question if SN 1994W destroyed its progenitor star.

3.2.3. Contrasting SN 2009ip and UGC 2773 OT2009-1

At $t = 0$ days, the temperature of UGC 2773 OT2009-1 is ∼7000 K (see Section 3.4), which is similar to the temperature during the classical "eruptive" state of LBVs (e.g., Humphreys & Davidson 1994). This contrasts with the higher temperature of 10,000 K derived for SN 2009ip (see Section 3.4), which lacks the narrow Fe-group absorption features, and is similar to other giant eruptions of LBVs (e.g., Humphreys et al. 1999). Many other LBV giant eruptions have temperatures similar to that of SN 2009ip (Humphreys & Davidson 1994). SN 2009ip was ∼2 mag brighter at peak than UGC 2773 OT2009-1, and SN 2009ip had a much larger increase in luminosity during the year before maximum than UGC 2773 OT2009-1, increasing by $\gtrsim$5 mag and ∼1 mag over 1 yr, respectively (S10). The fast-moving ejecta of SN 2009ip also contrasts with the relatively slow outflow of UGC 2773 OT2009-1.

The photometric and spectroscopic differences of these objects suggest different physical mechanisms. Clearly a supersonic explosion is necessary to produce the high-velocity

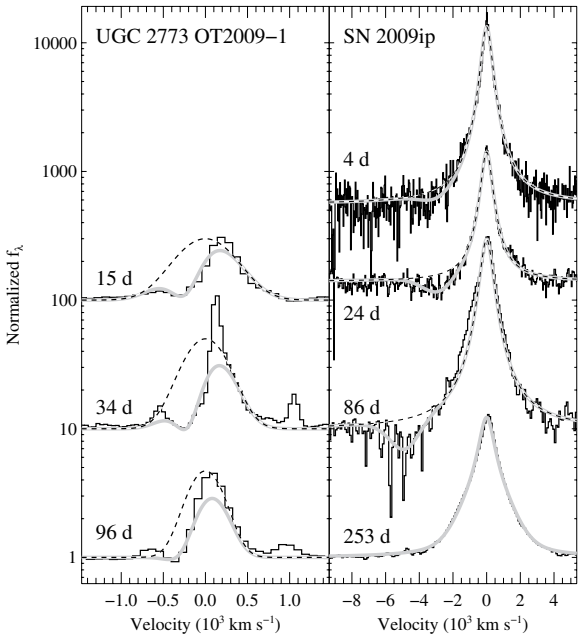

Figure 6. Normalized spectra of UGC 2773 OT2009-1 and SN 2009ip near Hα. The line profiles are fit with Gaussian and Lorentzian profiles, respectively. A profile fit to the redshifted portion of each profile is shown as a dashed line. For all spectra except for the 253 day spectrum of SN 2009ip, the gray lines correspond to the redshifted profile with a Gaussian absorption component added. For the 253 day spectrum of SN 2009ip, the gray line corresponds to a combination of Lorentzian and Gaussian emission components. Narrow [N II] can be seen in the spectrum of UGC 2773 OT2009-1.

absorption features of SN 2009ip, while UGC 2773 OT2009-1 shows no indication of an explosion. The differences in temperature and luminosity increase are also indicative of more energy injection (per unit mass) for SN 2009ip. A plausible explanation is that SN 2009ip is an LBV giant eruption triggered by an explosion, while UGC 2773 OT2009-1 is a particularly luminous S Dor-like classical LBV eruption.

3.3. Line Profiles

In this section, we examine the line profiles of Hα and Ca lines. These features provide an indication of the kinematics of the emitting material. The narrow lines are a tracer of the preshock circumstellar material, while the high-velocity absorption features in the spectra of SN 2009ip probe the outburst ejecta.

3.3.1. Hα

In Figure 6, we present the Hα line profiles of UGC 2773 OT2009-1 and SN 2009ip. Three separate epochs are shown for each object. Both objects have asymmetric line profiles. There are absorption components at about -350 km s^{-1} for UGC 2773 OT2009-1 and between -3000 and -6000 km s^{-1} for SN 2009ip. The line profile of SN 2009ip has a different shape and is much broader than that of UGC 2773 OT2009-1. We have attempted to fit these line profiles, but because of the asymmetry of the profiles, we first fit only the redshifted portion of each line profile and then add an absorption component to reproduce the blueshifted profile.

For the 15 day spectrum of UGC 2773 OT2009-1, we fit a Gaussian with FWHM $=$ 780 km s^{-1} to the red side of the feature. This value is twice that of the value found by S10 for a spectrum from day 22. Our spectrum is much lower resolution than that of the spectrum presented by S10, and we are not able to properly resolve the narrow emission in our spectrum. Therefore, the width of the line at this epoch is probably lower than our measured value. The 34 day spectrum of UGC 2773 OT2009-1 is contaminated by host-galaxy emission lines, making a fit to the inner regions of the line profile problematic. Ignoring this region, we were able to fit the redshifted portion of the line profile with a single Gaussian with FWHM $=$ 590 km s^{-1}. The 96 day spectrum has lower resolution, but is successfully fit by a Gaussian profile with FWHM $=$ 470 km s^{-1}.

To account for the asymmetric profile, we add an absorption component to the Gaussian line profiles. Fitting the full profile with two Gaussian functions, the emission component fit to the red side of the line and the absorption component added to fit the blue side of the line, we find absorption minima at -180, -110, and -80 km s^{-1} for the 15, 34, and 96 day spectra, respectively. This is different from the value of the actual minimum (-350 km s^{-1}) since the relatively strong emission masks the true minimum. S10 uses the observed minimum (-350 km s^{-1}) as the wind outflow velocity for UGC 2773 OT2009-1, while we suggest that it is slightly slower. Regardless, their conclusion that the velocity is consistent with the winds of blue supergiants, LBVs, and classical LBV eruptions still stands even with this lower velocity.

The line profiles of the first two spectra (days 4 and 24) of SN 2009ip are well fit by Lorentzian profiles with FWHM $=$ 780 km s^{-1} and the third is best fit by a Lorentzian profile with FWHM $=$ 890 km s^{-1}, which are larger than that found by S10, 550 km s^{-1}. A Lorentzian profile of 550 km s^{-1} is not a particularly bad fit to our data, but we find that the larger velocities better represent the data. One can also see in Figure 8 of S10, that the 550 km s^{-1} Lorentzian slightly underpredicts the true FWHM of the line, so the data appear to be consistent.

In the 24 day spectrum of SN 2009ip, we see an absorption feature with a minimum at a velocity of about -3000 km s^{-1}. (This high-velocity absorption is seen for all Balmer lines with varying instrument configurations and on two epochs; see Section 3.2.1.) This feature is well fit by including a Gaussian absorption component with a minimum at -2800 km s^{-1}. Adding a component with this velocity also improves the fit to the 4 day Hα profile slightly, but not in a significant way. The 86 day spectrum shows an even *stronger* high-velocity absorption component with the minimum of the absorption at a *larger* velocity of -4800 km s^{-1}. The blue wing of the absorption component, representing the fastest moving material, corresponds to a velocity of about -4500 and -7000 km s^{-1} for the 24 and 86 day spectra, respectively.

These velocities are much larger than the wind speed of LBVs and are larger than the measured velocity for any LBV eruption with the exception of the 1843 eruption of η Car, which had some material expelled at 3000–6000 km s^{-1} (Smith 2008). The velocities measured for SN 2009ip are similar to that of the ejecta of typical core-collapse SNe (such as SN 1998S; see Figure 4 and Section 3.2.1) and are somewhat similar to that of Wolf-Rayet winds (e.g., Abbott & Conti 1987). S10 concurrently discovered this high-velocity material and arrived at similar conclusions. We discuss the implications of these features in Section 4.2.

The 253 day spectrum of SN 2009ip does not contain an absorption component, which is probably the result of the ejecta becoming nebular. The emission component is very wide with an FWHM $\approx$ 1000 km s^{-1}. It cannot be well fit by only a Lorentzian or Gaussian profile, but a combination of the two

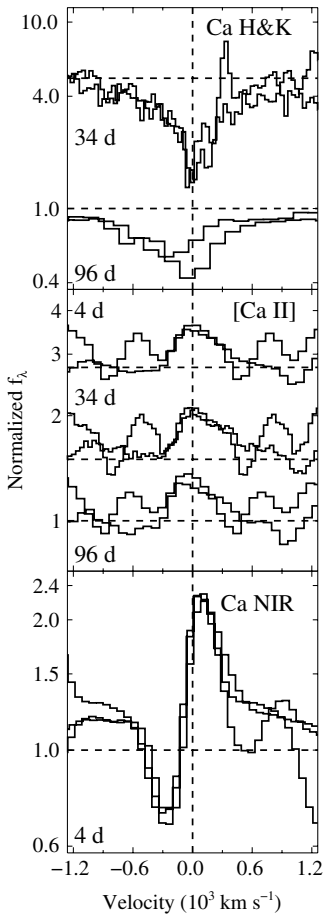

Figure 7. Normalized spectra of UGC 2773 OT2009-1 near Ca H&K (top), [Ca II] λλ7291, 7325 (middle), and Ca II NIR triplet (bottom). Dashed lines indicate the continuum flux and zero velocity for each line. Each member of the multiplet is overplotted for a given spectrum.

provides an excellent fit. Our best fit consists of a Lorentzian profile with FWHM = 1060 km s^{-1} and a Gaussian profile with FWHM = 2750 km s^{-1}; however, we caution that this fit is not strictly unique, and there may be an unresolved narrow component that affects the profile. Regardless, the high velocities of the emission component at late time further suggest fast-moving ejecta.

3.3.2. Permitted and Forbidden Ca II

Only our first and last spectra of SN 2009ip cover the Ca II NIR triplet, and no spectrum shows obvious [Ca II] λλ7291, 7325 lines, similar to the spectra presented by S10. Furthermore, the Ca H&K lines are confused by the strong Balmer sequence in SN 2009ip. Because of these factors, it is difficult to evaluate the characteristics of the Ca II behavior in this object (other than the absent [Ca II] lines).

UGC 2773 OT2009-1, on the other hand, has strong Ca II features. This can be seen in Figure 2. We examine the Ca H&K, [Ca II] λλ7291, 7325, and Ca II NIR triplet line profiles in Figure 7. The Ca H&K lines show a broad absorption extending from −1000 to +500 km s^{-1} and a minimum at about −50 km s^{-1} that does not appear to change significantly between the two epochs. Each component of the Ca II NIR triplet shows a strong P-Cygni profile with a minimum at approximately −250 km s^{-1}, slightly larger than the minima of Ca H&K.

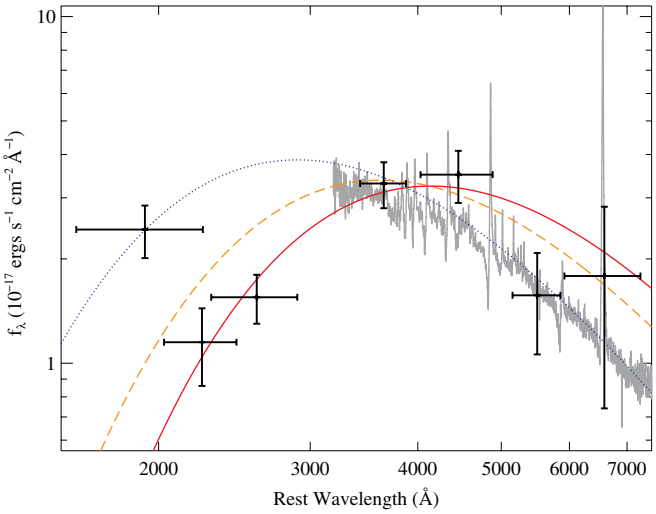

Figure 8. UV/Optical photometry of SN 2009ip during the fading event immediately after maximum brightness. The blue dotted, orange dashed, and red solid curves correspond to 10,000, 8000, and 7000 K blackbody spectra, respectively. The 23 day spectrum is also plotted to show the consistency with both the photometry and the 10,000 K blackbody. All photometry is consistent with the 8000 and 10,000 K blackbody spectra. Ignoring the bluest (UVW2) filter, the data are also consistent with the 7000 K blackbody.

(A color version of this figure is available in the online journal.)

The [Ca II] λλ7291, 7325 lines are visible in all epochs of our spectroscopy. We confirm the additional line between this doublet seen by S10 and identify this as Fe II λ7308. Both [Ca II] lines have asymmetric profiles in all spectra; the peak is at zero velocity, but the emission extends further to the red than to the blue. The lines from all epochs have FWHMs of ∼400 km s^{-1}, which is about half the width of Hα (see Section 3.3.1), similar to that found for NGC 300 OT2008-1 (Berger et al. 2009b).

3.4. Spectral Energy Distribution and Dust Emission

Using our available photometry and spectroscopy, we can examine the SED of both objects. We have only optical spectra of SN 2009ip, which limits our ability to examine multiple blackbody components for this object. A 10,000 K blackbody fits our optical spectra well, which is consistent with that found by S10.

Our single epoch of *Swift* photometry occurred during the dramatic fading of the light curve immediately following maximum brightness (S10). In Figure 8, the *Swift* photometry is combined with the unfiltered photometry (approximately *R* band) of S10 (with an uncertainty of 0.5 mag to account for the 16 hr difference in the epoch of the observations) during the minimum. We overplot the 23 day spectrum for comparison. The optical photometry is consistent with the optical spectrum and a 10,000 K blackbody (modulo emission lines). The UVW2 flux is also consistent with this blackbody, however, the UVM2 and UVW1 measurements fall well below this curve. Although this may be the result of line blanketing, these data are also consistent with a blackbody curve with a temperature as low as 8000 K. If we ignore the UVW2 measurement, the data can be fit by a 7000 K blackbody. Although our data suggest a possible change in the SED during the fading event, the lack of necessary comparison UV data from a different epoch prevent a clear indication of a change.

Using the 15 day optical spectrum and 22 day NIR spectrum, we are able to examine the SED of UGC 2773 OT2009-1 over nearly a decade in wavelength. Between these dates, the

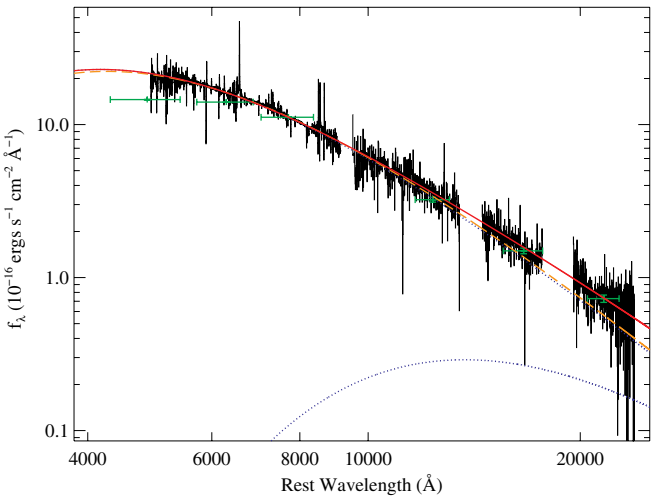

Figure 9. Optical/NIR spectrum of UGC 2773 OT2009-1. Single (6800 K; dashed orange line) and double (2100 and 6900 K; solid red line) blackbody fits to the spectrum are overplotted. The individual components of the double blackbody fit are shown as blue dotted lines. The double blackbody is a better fit to the data than the single blackbody. Green points show our photometry, which also shows a NIR excess. The *g*-band flux is below that of either curve, but that is likely the result of line blanketing.

(A color version of this figure is available in the online journal.)

light curve of UGC 2773 OT2009-1 was essentially constant, having the same magnitude (within 1σ; S10). Using the long wavelengths of the NIR spectrum, our data are sensitive to any relatively low temperature thermal components.

We fit a single blackbody to these data, ignoring regions with strong line features and simultaneously fitting the scaling between the optical and NIR spectra. Doing this results in a best-fit temperature of 6800 K. This single blackbody consistently underpredicts the flux at NIR wavelengths. As a result, we have also attempted to fix the spectrum with a double blackbody model. This model, which produces a much better fit, results with temperatures $T_1 = 6950$ K and $T_2 = 2100$ K. The full spectrum and associated fits are shown in Figure 9. Although a dust emission spectrum would slightly deviate from a blackbody, a blackbody is a reasonable approximation (e.g., Smith et al. 2008), although the blackbody temperature usually overestimates the true dust temperature by up to 20% (e.g., Nozawa et al. 2008).

The NIR SED can also be reasonably fit by free–free emission, which would be produced if there is a significant stellar wind. However, the flux from this emission would require a sustained mass-loss rate of $\dot{M} \approx 10^{-3}\,M_\odot$ yr^{-1}, which is an order of magnitude larger than that of typical LBVs in a short-lived shell ejection phase (Humphreys & Davidson 1994). It is therefore unlikely that free–free emission is dominating the NIR emission.

S10 noted that UGC 2773 OT2009-1 had a (photometric) NIR excess, but could not distinguish between circumstellar extinction and dust emission. To test the former case, we attempted to fit the spectrum with a single blackbody, but with an additional extinction term. With R_V fixed to 3.1, this model did not fit the data well. The model was able to sufficiently reproduce the data if we allowed $R_V < 1$, which is unphysical. We therefore conclude that the NIR excess is likely due to dust emission.

Scaling our spectrum to our broadband photometry, we can calibrate the blackbody flux, which in turn constrains the ratio R/D, where R is the radius of the blackbody radiation and D is the distance to the object. Using $D = 6 \pm 0.5$ Mpc, we find that the hot and cool blackbodies have radii of $(1.50 \pm 0.16) \times 10^{14}$ cm and $(4.3 \pm 0.4) \times 10^{14}$ cm (13.0 ± 1.1 AU and 29 ± 2 AU), respectively. The size of the cool emitting region is of the same order of magnitude of the size of the Homunculus nebula surrounding η Car, but about an order of magnitude smaller than the pre-outburst dust radii of NGC 300 OT2008-1 (330 AU; Prieto et al. 2009; Berger et al. 2009b) and SN 2008S (80-160 AU; Berger et al. 2009b; Prieto et al. 2009; Wesson et al. 2009).

Following the prescription outlined by Smith et al. (2008 and references therein), we can measure the mass of the emitting dust. Specifically,

$$M_d = 1.08 \times 10^{-8} \rho \left(\frac{R_d}{10^{14}\ \mathrm{cm}}\right)^2 \left(\frac{T_d}{1000\ \mathrm{K}}\right)^{-2} M_\odot, \quad (1)$$

where M_d is the dust mass, R_d is the radius of the dust, T_d is the dust temperature, and ρ is the dust density. For the values obtained from the spectra, $T_d = 2100$ K and $R_d = 4.3 \times 10^{14}$ cm, and assuming a dust grain density of $\rho = 2.25$ g cm^{-3}, we find a dust mass of $M_d \approx 1 \times 10^{-8}\,M_\odot$. Since there could be a significant amount of dust emission at lower temperatures, this is a lower limit on the total dust mass; however, it is worth noting that this measurement is orders of magnitude less than the dust created in some SNe (e.g., Kotak et al. 2009 and references therein). We note depending on the dust composition, the dust temperature may differ from the blackbody temperature by hundreds of degrees.

The dust is very close to the star and its temperature is near the limit of grain survival. Additionally, the blackbody fits indicate that the cooler component is outside the hot component, which presumably comes from the outburst ejecta. Given these conditions, it is very likely that pre-existing circumstellar dust was heated and is emitting as it is being vaporized, rather than newly formed post-shock dust emitting as it cools.

4. DISCUSSION

UGC 2773 OT2009-1 and SN 2009ip provide excellent examples of the diversity of massive star outbursts. The discussion by S10 also detail the similarities and highlight the differences of these objects. Although there are a few minor differences between our analysis and that of S10, the main conclusions are similar. We provide similar mass estimates for the progenitor stars and have obtained similar optical spectroscopy. S10 provided a historical light curve of the events and detailed light curves after outburst. We provide NIR spectroscopy and additional spectroscopy, which provided useful information regarding the circumstellar dust of UGC 2773 OT2009-1 (Section 3.4) and the "reverse Hubble law" for the high-velocity ejecta of SN 2009ip (see Section 4.2). In the following sections, we review our findings (and those of S10) and discuss the implications of our observations.

4.1. Different Massive Star Outbursts

UGC 2773 OT2009-1 increased its optical brightness by $\sim$1 mag during outburst and has a cool spectrum with many narrow absorption lines and [Ca II] emission. It occurred near a star cluster containing stars with initial masses of $\sim 25\,M_\odot$ and shows evidence for a very cool ($T \approx 2100$ K) thermal component that is radiated by circumstellar dust. SN 2009ip had a more massive and relatively isolated progenitor. At peak,

it had risen at least 4 mag over the previous year, and its spectrum was hot and dominated by H Balmer emission lines. After having a significant fading and rebrightening over three weeks, it developed high-velocity absorption lines. Its SED is consistent with no dust emission.

The high temperature and large increase in optical luminosity for SN 2009ip indicates that it was a true giant eruption akin to the 1843 eruption of η Car. UGC 2773 OT2009-1, on the other hand, has spectral characteristics similar to that of S Dor at maximum. Although UGC 2773 OT2009-1 brightened by $\sim$5 mag (including the current eruption) over the last 10 years (Section 2; see also S10), which is significantly larger than the largest normal variation of S Dor stars ($\sim$3 mag; van Genderen 2001), its optical luminosity did not increase as much as typical giant eruptions. Part of the increase in optical luminosity is probably the result of dust destruction, which would increase the optical luminosity while keeping the bolometric luminosity constant and not affecting the spectral type. In this case, UGC 2773 OT2009-1 would be more similar to typical LBV variability, but the presence of circumstellar dust (which is destroyed during the event) makes the optical variability larger than that of other LBVs undergoing a similar event.

The outbursts of NGC 300 OT2008-1 and SN 2008S both had relatively low-temperature SEDs (Berger et al. 2009b), but neither had the forest of absorption lines found in UGC 2773 OT2009-1. All three objects had [Ca II] emission, but as suggested by S10, this may be linked to the circumstellar environment, and particularly dust destruction, rather than the event. Our observations have shown that there is dust in the circumstellar environment of the progenitor, and that it was likely pre-existing dust that is in the process of being vaporized. Additionally, SN 1999bw had [Ca II] emission (Garnavich et al. 1999) and had an IR excess consistent with dust emission at late times (Sugerman et al. 2004). All four massive star outbursts with observed [Ca II] emission (SN 1999bw, SN 2008S, NGC 300 OT2008-1, and UGC 2773 OT2009-1) have evidence of circumstellar dust. We do note that SN 2000ch had a $\sim$7000 K spectrum and an infrared excess consistent with dust emission, but no strong [Ca II] emission was detected in the relatively low signal-to-noise spectra presented by Wagner et al. (2004). It is therefore possible to have a cool object and circumstellar dust yet not have strong [Ca II] emission. Although all objects with [Ca II] emission show evidence for circumstellar dust, it is possible to have [Ca II] emission without any connection to circumstellar dust, so the presence of this feature may not be perfectly correlated with the existence of circumstellar dust.

Although UGC 2773 OT2009-1, NGC 300 OT2008-1, and SN 2008S have circumstellar dust and similar temperatures, other than the narrow H Balmer and [Ca II] (which we link to the presence of circumstellar dust) emission, the spectra and progenitors are not particularly similar. Particularly, NGC 300 OT2008-1 and SN 2008S had relatively featureless spectra and progenitors with initial masses of 10–25 $M_{\odot}$, while UGC 2773 OT2009-1 had a spectrum dominated by narrow lines and a more massive progenitor ($\gtrsim$25 $M_{\odot}$). Further contrasting these events, while NGC 300 OT2008-1 and SN 2008S had relatively fast declining light curve after maximum (Bond et al. 2009; Smith et al. 2009), UGC 2773 OT2009-1 has a relatively flat light curve near maximum (S10). Additional data are necessary to determine if the outburst mechanisms in these objects are similar.

Using SN 2009ip and UGC 2773 OT2009-1 as examples, there appears to be two distinct elements that determine the observational properties of massive star outbursts. The first is the temperature of the outburst, which may be related to the increase in luminosity, the instability that causes the eruption, the width of the emission lines, and possibly the energetics of the outburst and if there is an explosion (see Section 4.2). This directly determines the shape of the optical SED, the ionization, if there is a forest of absorption lines, and possibly the shape of the line profiles, if there is high-velocity absorption. The other characteristic is the amount of circumstellar dust, which may cause strong Ca emission (and particularly [Ca II] emission) and will determine the shape of the SED at longer wavelengths. UGC 2773 OT2009-1 and SN 2009ip would occupy very different regions of the parameter space created by these two dimensions. NGC 300 OT2008-1 and SN 2008S would be close to UGC 2773 OT2009-1, while LBV giant eruptions such as SN 1997bs would be close to SN 2009ip. Alternatively, Kashi et al. (2010) suggested that NGC 300 OT2008-1 was more similar to an LBV giant eruption.

It remains to be seen if there are hot massive star outbursts with a large amount of circumstellar dust or if there are cool massive star outbursts with little circumstellar dust. η Car has 0.125 $M_{\odot}$ of dust surrounding it (Smith et al. 2003); if it were to have another giant eruption today, would it be cool? SN 1999bw had [Ca II] emission and displayed dust emission at late times, was it hot? An IR survey of recent massive star outbursts with good spectroscopic coverage may provide these answers. In the future, optical and NIR observations may be sufficient to determine these characteristics for other massive star outbursts.

4.2. SN 2009ip: A Supersonic Explosion

The spectra of SN 2009ip have absorption attributed to high-velocity (up to $\sim$7000 km s^{-1}) material (see Section 3.3.1; S10). Contrary to what is expected from a single outburst or explosion, the velocity of the absorption feature increases with time. In a typical SN, the ejecta naturally follow a Hubble law with the highest velocity material being the most distant from the explosion site. Spectral lines have a blueshifted absorption due to the scattering processes in the photosphere of the SN. Low velocity material is hidden behind the photosphere, only to be revealed at later times. As the photosphere recedes, the highest-velocity material becomes optically thin, resulting in the blueshifted velocity of a spectral line to decrease with time. Since the absorbing material must be at just slightly larger radii than the photosphere, the high-velocity material must have been ejected during the eruption. (If the absorbing material were from a previous eruption, the ejecta from the more recent eruption would have had to be moving even faster.)

It is possible that the high-velocity absorption is a component of P-Cygni features from the ejected material. The Lorentzian profile slightly underestimates the emission flux in the 86 day spectrum (see Figure 6), which may be the result of P-Cygni emission contributing to the line. Since the high-velocity absorption is coming from the ejecta, the outburst of SN 2009ip must have been extremely energetic, expelling a large amount of material at very high velocities. However, for the velocity to *increase* with time, either the ejecta must not follow a Hubble expansion or the radius of the photosphere (in velocity space) must somehow increase with time.

In a single explosion, the ejecta naturally follow a Hubble law; however, multiple explosions can change the velocity profile of the ejecta. If two explosions occurred in short succession, one can produce the inverted velocity gradient seen in SN 2009ip. In this toy model, the photosphere would recede into the ejecta

of the first explosion, but at some point the fastest-moving ejecta of the second explosion would overtake the photosphere, increasing the velocity. If there are no other explosions, the velocity of the absorption would decrease from there.

The photometric behavior of SN 2009ip is consistent with this picture. The first explosion would produce the fast rise to maximum. As noted by S10, the timescale of the fading is much shorter than the timescales for many physical processes such as dust extinction.[15] This behavior is very similar to that of SN 2000ch, which brightened by 2.1 mag in 9 days to maximum, then immediately faded by 3.4 mag in 7 days, immediately followed by a 2.2 mag rise in 4 days, after which the magnitude stayed relatively constant (Wagner et al. 2004). Spectra of SN 2000ch taken during the fading and on its plateau show no strong evidence for high-velocity ejecta, but the spectra may not be of high enough quality to see these features.

S10 hypothesized that rapid fading may have been caused by an optically thick shell being ejected after the first outburst. If this process did occur in SN 2009ip, then there are several implications: (1) the velocity of the absorption should eventually decrease, (2) the interaction of the ejecta from the two explosions could be a significant source of X-ray and radio emission, and (3) the X-rays might excite certain elements producing high-excitation lines such as He II in optical spectra. Our X-ray limit of $L_X < 4.8 \times 10^{38}$ erg s^{-1} taken during the minimum is not particularly constraining. We do not detect any He II λ4686 emission in the 4 or 24 day spectra; however, there is a low significance detection of a line consistent with He II λ4686 emission in the 86 day spectrum. Additional spectroscopy is necessary to determine the late-time velocity gradient.

5. CONCLUSIONS

We have presented extensive UV, optical, and NIR data for two transients, SN 2009ip and UGC 2773 OT2009-1. Although these events appear to be similar phenomena (luminous outbursts of massive stars), the details of the events show that there are many differences. These differences provide examples of the diversity of such events.

A previous study of these events, S10, provided an initial analysis of the object. Although the two studies agree on most points, our interpretation of the entire data set is somewhat different than that of S10. In particular, we agree that based on pre-outburst *HST* imaging, historical light curves, and outburst spectroscopy, the progenitors of SN 2009ip and UGC 2773 OT2009-1 exhibit all properties of LBVs with masses of $\gtrsim$60 and $\gtrsim$25 $M_\odot$, respectively. If there were a significant amount of circumstellar dust surrounding the progenitor of UGC 2773 OT2009-1, then it might have been much more massive. We also agree that the spectra of the two events are significantly different, but consistent with known LBVs or LBV outbursts. While UGC 2773 OT2009-1 had a cooler spectrum with a forest of absorption lines reminiscent of an F-type supergiant (similar to S Dor in its high state), SN 2009ip had a hot spectrum and exhibited mainly H Balmer emission (similar to other LBV giant eruptions). The spectral characteristics (particularly [Ca II] emission) and circumstellar dust link UGC 2773 OT2009-1 to the lower-mass, dust-obscured progenitors of NGC 300 OT2008-1 and SN 2008S. We agree that the progenitors of these objects are all massive stars and may have many characteristics similar to those of the LBV class, which could extend the mass range for LBV-like activity to relatively low mass stars.

However, there are distinct differences between the analyses of S10 and of that presented here. Specifically, the initial mass ranges for the progenitors are slightly different in the two studies, with S10 estimating 50–80 $M_\odot$ (instead of $\gtrsim$60 $M_\odot$) and $\gtrsim$20 $M_\odot$ (instead of $\gtrsim$25 $M_\odot$) for SN 2009ip and UGC 2773 OT2009-1, respectively. The differences lie in the conversion from *HST* filters to Bessell filters and the adapted color range for the progenitor of SN 2009ip, and the additional information provided by stars in the vicinity of the progenitor of UGC 2773 OT2009-1. Clearly these differences are minor and do not affect our results.

Our interpretation of the exact nature of UGC 2773 OT2009-1 differs from that of S10. While S10 contends that this object is a true giant eruption of an LBV, we question this assertion and propose that it may be the result of extreme S Dor variability combined with circumstellar dust destruction.

While S10 found an NIR excess for UGC 2773 OT2009-1, hypothesizing that there may be dust emission as it is vaporized, we find more conclusive evidence for this scenario through our NIR spectroscopy. The NIR spectrum is consistent with an additional blackbody with $T \approx 2100$ K, but is inconsistent with reddening by dust. The presence of this dust indicates that the initial mass estimate of the progenitor (based on optical *HST* imaging) is a lower limit, and that the true initial mass is likely much larger.

In addition to what was discussed by S10, we have also detected high-velocity absorption in the spectra of SN 2009ip, indicative of an explosion (as opposed to subsonic outburst). The absorption has an inverse velocity gradient suggesting multiple explosions in short succession. The rapid fading and brightening shortly after maximum brightness noted by (S10) is consistent with multiple explosions, where a second explosion ejects an optically thick shell that temporarily dims the object.

We also note the spectroscopic similarity of UGC 2773 OT2009-1 and SN 1994W, which Dessart et al. (2009) has previously suggested was not a true SN that destroyed its progenitor star.

SN 2009ip and UGC 2773 OT2009-1 are very different manifestations of a similar phenomenon: extreme brightening of massive stars. With these objects and similar events (such as η Car, NGC 300 OT2008-1, and SNe 1961V, 1954J, 1997bs, 2000ch, 2002kg, and 2008S), we show that luminous outbursts of massive stars are very heterogeneous. Some of this diversity is likely linked to the instability that causes the eruption, while some is caused by the circumstellar environment. Additional observations of new massive star eruptions are necessary to determine the physical mechanisms of the eruptions, the content of the circumstellar environments, and whether the two are physically connected.

R.J.F. is supported by a Clay Fellowship. O.D.F. is grateful for support from NASA GSRP, ARCS, and VSGC. E.M.L. is supported in part by a Ford Foundation Predoctoral Fellowship.

We thank A. Miller for clarification of our dust mass estimate. We are indebted to the staffs at the APO, Gemini, Magellan, and MMT Observatories for their dedicated services. We kindly thank Y. Shen, X., Liu, M. Strauss, K. Olsen, and R. McDermid for obtaining some of the data presented in the paper. We thank

[15] The calculation by (S10) for the time until dust formation for SN 2009ip assumes a velocity of 500 km s^{-1}. Although the ejecta are moving much faster than this assumed value, they would need to have a velocity of $\gtrsim$20,000 km s^{-1} to reach the sublimation radius at the time of fading.

R. Chornock, R. Humphreys, and R. Kirshner for stimulating discussions about the transients.

This study is based on observations made with the NASA/ESA *Hubble Space Telescope*, obtained from the data archive at the Space Telescope Science Institute. STScI is operated by the Association of Universities for Research in Astronomy, Inc., under NASA contract NAS 5-26555. Based in part on observations obtained at the Gemini Observatory, which is operated by the Association of Universities for Research in Astronomy, Inc., under a cooperative agreement with the US National Science Foundation on behalf of the Gemini partnership: the NSF (United States), the Science and Technology Facilities Council (United Kingdom), the National Research Council (Canada), CONICYT (Chile), the Australian Research Council (Australia), Ministério da Ciência e Tecnologia (Brazil), and Ministerio de Ciencia, Tecnología e Innovación Productiva (Argentina); the 6.5 m Magellan Telescopes located at Las Campanas Observatory, Chile; the MMT Observatory, a joint facility of the Smithsonian Institution and the University of Arizona; the Fan Mountain Observatory 0.8 m telescope; and the Apache Point Observatory 3.5 m telescope, which is owned and operated by the Astrophysical Research Consortium. We acknowledge the use of public data from the *Swift* data archive.

Facilities: ARC (TripleSpec), FMO:31in (FanCam), Gemini:Gillett (GMOS), *HST* (WFPC2), Magellan:Baade (IMACS), Magellan:Clay (MagE), MMT (Blue Channel), *Swift* (UVOT, XRT)

REFERENCES

Abbott, D. C., & Conti, P. S. 1987, ARA&A, 25, 113
Ball, L., Campbell-Wilson, D., Crawford, D. F., & Turtle, A. J. 1995, ApJ, 453, 864
Berger, E., & Foley, R. J. 2009, ATel, 2187, 1
Berger, E., Foley, R. J., & Ivans, I. 2009a, ATel, 2184, 1
Berger, E., et al. 2009b, ApJ, 699, 1850
Blondin, S., et al. 2006, AJ, 131, 1648
Boles, T. 2009, CBET, 1931, 1
Bond, H. E., Bedin, L. R., Bonanos, A. Z., Humphreys, R. M., Monard, L. A. G. B., Prieto, J. L., & Walter, F. M. 2009, ApJ, 695, L154
Botticella, M. T., et al. 2009, MNRAS, 398, 1041
Chu, Y., Gruendl, R. A., Stockdale, C. J., Rupen, M. P., Cowan, J. J., & Teare, S. W. 2004, AJ, 127, 2850
Chugai, N. N., et al. 2004, MNRAS, 352, 1213
Cushing, M. C., Vacca, W. D., & Rayner, J. T. 2004, PASP, 116, 362
Dessart, L., Hillier, D. J., Gezari, S., Basa, S., & Matheson, T. 2009, MNRAS, 394, 21
Dolphin, A. E. 2000, PASP, 112, 1383
Filippenko, A. V., Barth, A. J., Bower, G. C., Ho, L. C., Stringfellow, G. S., Goodrich, R. W., & Porter, A. C. 1995, AJ, 110, 2261
Foley, R. J., et al. 2009, AJ, 138, 376
Foley, R. J., et al. 2003, PASP, 115, 1220
Foley, R. J., et al. 2006, ApJ, 645, 450
Frew, D. J. 2004, J. Astron. Data, 10, 6
Garnavich, P., Jha, S., Kirshner, R., Calkins, M., & Brown, W. 1999, IAU Circ., 7150, 1
Gogarten, S. M., Dalcanton, J. J., Murphy, J. W., Williams, B. F., Gilbert, K., & Dolphin, A. 2009, ApJ, 703, 300
Goodrich, R. W., Stringfellow, G. S., Penrod, G. D., & Filippenko, A. V. 1989, ApJ, 342, 908
Herter, T. L., et al. 2008, Proc. SPIE, 7014, 70140X
Hook, I. M., Jørgensen, I., Allington-Smith, J. R., Davies, R. L., Metcalfe, N., Murowinski, R. G., & Crampton, D. 2004, PASP, 116, 425
Horne, K. 1986, PASP, 98, 609
Humphreys, R. M., & Davidson, K. 1994, PASP, 106, 1025
Humphreys, R. M., Davidson, K., & Smith, N. 1999, PASP, 111, 1124
Humphreys, R. M., Davidson, K., & Smith, N. 2002, AJ, 124, 1026
Jones, T. J., et al. 1993, ApJ, 411, 323
Kanneganti, S., Park, C., Skrutskie, M. F., Wilson, J. C., Nelson, M. J., Smith, A. W., & Lam, C. R. 2009, PASP, 121, 885
Kashi, A., Frankowski, A., & Soker, N. 2010, ApJ, 709, L11
Kelson, D. D. 2003, PASP, 115, 688
Kotak, R., et al. 2009, ApJ, 704, 306
Leonard, D. C., Filippenko, A. V., Barth, A. J., & Matheson, T. 2000, ApJ, 536, 239
Marshall, J. L., et al. 2008, Proc. SPIE, 7014, 701454
Massey, P. 2000, PASP, 112, 144
Maund, J. R., et al. 2006, MNRAS, 369, 390
Maza, J., et al. 2009, CBET, 1928, 1
Miller, A. A., Li, W., Nugent, P. E., Bloom, J. S., Filippenko, A. V., & Merritt, A. T. 2009, ATel, 2183, 1
Mould, J. R., et al. 2000, ApJ, 529, 786
Nozawa, T., et al. 2008, ApJ, 684, 1343
Prieto, J. L. 2008, ATel, 1550, 1
Prieto, J. L., Sellgren, K., Thompson, T. A., & Kochanek, C. S. 2009, ApJ, 705, 1425
Prieto, J. L., et al. 2008, ApJ, 681, L9
Schaller, G., Schaerer, D., Meynet, G., & Maeder, A. 1992, A&AS, 96, 269
Schlegel, D. J., Finkbeiner, D. P., & Davis, M. 1998, ApJ, 500, 525
Schmidt, G. D., Weymann, R. J., & Foltz, C. B. 1989, PASP, 101, 713
Schultz, G. V., & Wiemer, W. 1975, A&A, 43, 133
Smith, N. 2008, Nature, 455, 201
Smith, N., Chornock, R., Silverman, J. M., Filippenko, A. V., & Foley, R. J. 2010, ApJ, 709, 856
Smith, N., Foley, R. J., & Filippenko, A. V. 2008, ApJ, 680, 568
Smith, N., Ganeshalingam, M., Li, W., Chornock, R., Steele, T. N., Silverman, J. M., Filippenko, A. V., & Mobberley, M. P. 2009, ApJ, 697, L49
Smith, N., Gehrz, R. D., Hinz, P. M., Hoffmann, W. F., Hora, J. L., Mamajek, E. E., & Meyer, M. R. 2003, AJ, 125, 1458
Smith, N., Humphreys, R. M., & Gehrz, R. D. 2001, PASP, 113, 692
Smith, N., et al. 2010, AJ, 139, 1451
Soderberg, A. M., et al. 2008, Nature, 453, 469
Sollerman, J., Cumming, R. J., & Lundqvist, P. 1998, ApJ, 493, 933
Stockdale, C. J., Rupen, M. P., Cowan, J. J., Chu, Y., & Jones, S. S. 2001, AJ, 122, 283
Sugerman, B., Meixner, M., Fabbri, J., & Barlow, M. 2004, IAU Circ., 8442, 2
Thompson, T. A., Prieto, J. L., Stanek, K. Z., Kistler, M. D., Beacom, J. F., & Kochanek, C. S. 2009, ApJ, 705, 1364
Van Dyk, S. D., Filippenko, A. V., Chornock, R., Li, W., & Challis, P. M. 2005, PASP, 117, 553
Van Dyk, S. D., Filippenko, A. V., & Li, W. 2002, PASP, 114, 700
Van Dyk, S. D., Li, W., Filippenko, A. V., Humphreys, R. M., Chornock, R., Foley, R., & Challis, P. M. 2006, arXiv:astro-ph/0603025
Van Dyk, S. D., Peng, C. Y., King, J. Y., Filippenko, A. V., Treffers, R. R., Li, W., & Richmond, M. W. 2000, PASP, 112, 1532
van Dyk, S. D., Weiler, K. W., Sramek, R. A., Schlegel, E. M., Filippenko, A. V., Panagia, N., & Leibundgut, B. 1996, AJ, 111, 1271
van Genderen, A. M. 2001, A&A, 366, 508
Wade, R. A., & Horne, K. 1988, ApJ, 324, 411
Wagner, R. M., et al. 2004, PASP, 116, 326
Weis, K., & Bomans, D. J. 2005, A&A, 429, L13
Wesson, R., et al. 2009, MNRAS, 1823
Wilson, J. C., et al. 2004, Proc. SPIE, 5492, 1295